X-ray analysis of Centaurus A

Bachelorarbeit aus der Physik

Vorgelegt von

Christina Gräfe

14. April 2014

Dr. Karl Remeis-Sternwarte Bamberg
Friedrich-Alexander-Universität Erlangen-Nürnberg

Betreuer:
Prof. Dr. Jörn Wilms
Prof. Dr. Matthias Kadler

Contents

Zusammenfassung

In meiner Bachelorarbeit zeige ich die Analysen zweier Röntgenbeobachtungen von Centaurus A, unserer nächsten aktiven Galaxie (AGN). Obwohl es in der Vergangenheit bereits mehrere Studien in allen Wellenlängenbereichen gab, ist die Quelle noch weit davon entfernt, komplett verstanden zu sein. In meiner Arbeit benutze ich Daten von *Chandra*/ACIS und *Suzaku*/XIS um die Röntgeneigenschaften von Centaurus A zwischen 0.5 keV und 10 keV zu untersuchen. Die Kombination von *Suzaku*'s guter Energieauflösung zur Analyse des Röntgenspektrums im Detail zusammen mit *Chandra*'s hervorragender räumlicher Auflösung zur Trennung der verschiedenen Emissionsregionen und Bestimmung des Ursprungs der weichen Röntgenstrahlen erlaubt es, die diffuse Emissionsregion von Centaurus A eingehend zu untersuchen. Ich habe verschiedene (unaufgelöste) Emissionslinien im Material, welches den AGN umgibt, gefunden. Außerdem habe ich festgestellt, dass harte Röntgenstrahlen nicht nur vom Bereich des Kerns sondern auch von der ausgedehnten Region um diesen herum emittiert werden. Das gesamte harte Röntgenspektrum ist sehr variabel, wobei die Ursache für diese Variabilität noch nicht gefunden ist.

Abstract

In this bachelor thesis I present the analyses of two X-ray observations of Centaurus A, which is our nearest active galactic nucleus (AGN). Although there have been various studies over all wavebands in the past, this source is still far from being completely understood. In my work I use data from *Chandra*/ACIS and from *Suzaku*/XIS to study the X-ray properties of Centaurus A between 0.5 keV and 10 keV. Using *Suzakus*'s good energy resolution to analyze the X-ray spectrum in detail combined with *Chandra*'s excellent spatial resolution to separate different emission regions and determine the origin of the soft X-rays, allows us to study the diffuse emission region of Centaurus A. I find several unresolved emission lines in the material surrounding the center of the AGN, and I detect hard X-rays being emitted not online from the core region, but also from the extended region around the center. The overall hard X-ray emission of Centaurus A is highly variable. However, the reason of this variability is not yet found.

1 Introduction

In this work, I explain a detailed analysis of the X-ray spectrum of Centaurus A in the 0.5-10 keV band. I give an overview of the characteristics of active galactic nuclei, their emission processes, and X-ray satellites which have been used for obtaining the data. I concentrate on the emission of Centaurus A's diffuse region, show the results of my analyses, and make suggestions for further investigations.

1.1 AGN

Active galactic nuclei (AGN) belong to the most thrilling class of objects which modern astrophysics tries to understand and which are still being investigated even after 6 decades (already found in the early 20th century, systematic research on AGN started in $\sim$ 1960 (Schneider, 2006)). They can produce vast luminosity in small volumes and radiate over a broad range of frequencies (Krolik, 1999). The generally accepted model for AGN assumes a supermassive black hole at the center of a galaxy which causes the formation of an accretion disk and the perpendicular launch of a collimated outflow of matter, called a jet. A torus obscures the system, when within the line of sight (Urry & Padovani, 1995).

The main source of distinction for active galaxies is in type 1 (broad line) and type 2 (narrow line) AGN by appearance of their optical emission lines. In galaxies with fast moving, hot gas we mainly find Doppler broadened emission lines, while in cold, low-velocity gas or behind absorbing material we find only narrow emission lines. These type 1 and type 2 AGN can be sub-divided into radio-quiet or radio-loud sources. Other interesting objects are so-called blazars, which show strong variability and seem to "blaze" their material directly at us. Although seemingly different at first sight, the AGN unification scheme explains all those phenomena with the same model which we look at from different directions (see Fig. 1.1, Urry & Padovani, 1995).

Table 1.1: AGN taxonomy (Urry & Padovani, 1995)

	Type 1	Type 2
Radio-quiet	Seyfert 1 radio-quiet Quasars	Seyfert 2
Radio-loud	BL Lac radio-loud Quasars OVV	Fanaroff-Riley I Fanaroff-Riley II

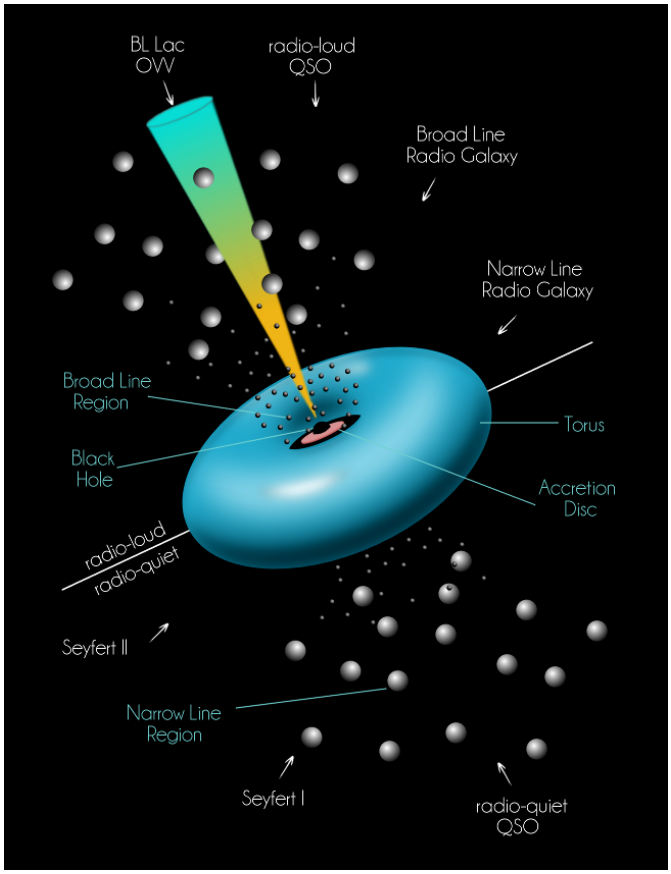

Figure 1.1: AGN unification model (Credit: Felicia Krauß after Urry & Padovani, 1995). The arrows indicate the different lines of sight, the "donut" marks a probable torus covering the innermost region of the AGN.

1.2 Accretion

AGN power by accreting material. Gas surrounding a black hole has an angular momentum, which is typically in the order of $\sim 6 \times 10^{28}\,\mathrm{cm^2 s^{-1}}$. In contrast, to keep a stable orbit, a black hole with a typical mass of $10^8\,M_\odot$ can only have an angular momentum of $1 \times 10^{24}\,\mathrm{cm^2 s^{-1}}$ (Krolik, 1999), which means the angular momentum of the surrounding material must decrease before it can be accreted. Friction and particle collisions (i.e., viscosity) are efficient ways to lose energy and hereby reducing angular momentum. This causes the material to fall inwards. Particles colliding while falling will eventually acquire the same angular momentum and consequently will orbit in the same plane, which we call an accretion disk (Krolik, 1999).

A mass m, falling from a radius $r + \Delta r$ to r, causes an energy release of

$$\Delta E \approx \frac{G m M_{\mathrm{BH}}}{r} \frac{\Delta r}{r}\,, \tag{1.1}$$

transforms half of this energy into thermal energy that is radiated locally, such that the associated luminosity is

$$\Delta L = \frac{G \dot{m} M_{\mathrm{BH}}}{2 r^2} \Delta r\,, \tag{1.2}$$

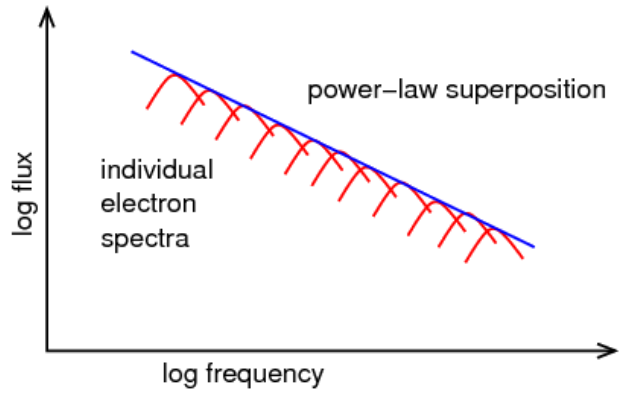

Figure 1.2: Synchrotron radiation as a superposition of electron distribution and energetic spectrum of single electrons. (Credit: Wilms, 2012 after Shu, 1991)

where $\dot{m}$ is the mass accretion rate. Given that the gravitational force of the black hole must be stronger than the radiation pressure if material is accreted, we find the Eddington limit, which is an upper limit of the mass accretion rate(Schneider, 2006):

$$\dot{M}_{\rm max} = \frac{L_{\rm Edd}}{\eta c^2} \,. \tag{1.3}$$

1.3 Emission mechanisms

1.3.1 Synchrotron radiation

Relativistic particles accelerated by a magnetic field emit synchrotron radiation and move along helical paths around the magnetic field lines. Their acceleration can be described by

$$m\gamma\frac{d\mathbf{v}}{dt} = \frac{q}{c}\mathbf{v}\times\mathbf{B} \text{ with } \gamma = \frac{1}{\sqrt{1-\frac{v^2}{c^2}}} \tag{1.4}$$

(Rybicki & Lightman, 1979). Both the spectral energy distribution of a single electron and the electron velocity distribution can be described with a powerlaw (Rybicki & Lightman, 1979, Wilms, 2012),

$$N(\gamma)d\gamma = \mathrm{C}\gamma^{-p}d\gamma \tag{1.5}$$

where equation 1.5 is an expression of the powerlaw distribution of electrons with energies between γ and $d\gamma$. For one electron, the spectral energy distribution is

$$P = \frac{4}{3}\sigma_{\rm T}c\beta^2\gamma^2\frac{B^2}{8\pi} \,, \tag{1.6}$$

where $\beta = v/c$ and $\sigma_{\rm T}$ is the Thomson cross section (Rybicki & Lightman, 1979). Thus, the observed spectrum again is a powerlaw given by the following equation:

$$P_{total} = \int P(\gamma)N(\gamma)d\gamma \tag{1.7}$$

1.3.2 Comptonization

When a photon collides with a non-relativistic electron, the photon energy decreases and its wavelength increases. This process is called Compton scattering and can be described by

$$\Delta\lambda = \lambda_c(1-\cos\theta) \text{ with } \lambda_c = \frac{h}{mc} = 0.02426\,\text{Å}\,. \tag{1.8}$$

If instead photons collide with electrons at relativistic speeds, the photons can gain energy and be scattered to shorter wavelengths, which is called inverse Compton effect (Rybicki & Lightman, 1979). A special case of the latter is Synchrotron Self-Compton scattering, where synchrotron photons are inverse Compton scattered by the same relativistic electrons, such that

$$\frac{P_{\text{synch}}}{P_{\text{compt}}} = \frac{U_B}{U_{\text{ph}}} \text{ with } U_B = \frac{B^2}{8\pi} \text{ and } U_{\text{ph}} = \int E\nu dE \tag{1.9}$$

with U_{ph} being the initial photon energy density (Rybicki & Lightman, 1979).

1.3.3 Ionization

When an electron in an atom (or ion) is hit by a photon or a free electron, it can be either brought into an excited state or even released, if the kinetic energy of the hitting particle is higher than the binding energy of the atomic shell

$$E_{\text{kin}} \geqslant h\nu - E_{\text{bind}}\,. \tag{1.10}$$

These two processes are called photoionization and collisional ionization. For collisional ionizaton, the cross section is given by

$$\sigma_{\text{coll}} = \frac{a n_s \ln(\frac{E_{\text{kin}}}{E_{\text{bind}}})}{E_{\text{kin}} E_{\text{bind}}} \quad \text{with} \quad a = 4.5\times10^{-24}\text{m}^2\text{keV}^2 \tag{1.11}$$

where n_s is the number of electrons in the shell and a the normalization (Kaastra et al., 2008). Considering the electron distribution for a thermal plasma, the number of ionizations if $kT \ll E_{\text{bind}}$ is given as

$$C_{\text{coll}} \simeq \left(\frac{2\sqrt{2}an_s}{\sqrt{\pi m_e}}\right)\frac{n_e n_i \sqrt{kT} e^{-E_{\text{bind}}/kT}}{E_{\text{bind}}^2} \tag{1.12}$$

and if $kT \gg E_{\text{bind}}$ as

$$C_{\text{coll}} \simeq \left(\frac{2\sqrt{2}an_s}{\sqrt{\pi m_e}}\right)\frac{n_e n_i \ln(kT/E_{\text{bind}})}{E_{\text{bind}}\sqrt{kT}}\,. \tag{1.13}$$

Therefore, the ionization rate is nearly zero at low temperatures (because here only few electrons have sufficient energy to ionize an atom) and at high temperatures as well (because of the small cross section at high energies, Kaastra et al. (2008)). For photoionization of hydrogen-like ions, the cross section is given by

$$\sigma_{\text{phot}} = \frac{64\pi n g(E,n)\alpha a_0^2}{3\sqrt{3}Z^2}\left(\frac{E_{\text{bind}}}{E_{\text{kin}}}\right)^3 \tag{1.14}$$

with n as the principal quantum number, α as the fine structure constant, a_0 as the Bohr radius and $g(E,n)$ as the Gaunt factor. For calculation of the latter, see Karzas & Latter (1961). The number of ionizations by photoionization is given by

$$C_{\text{phot}} = c \int_0^\infty n_{\text{i}} \sigma_{\text{phot}}(E) F(E) \mathrm{d}E \tag{1.15}$$

where $F(E)$ is the ionizing spectrum.

1.3.4 Fluorescence

Iron fluorescence is most important for X-ray observations of AGN. An ionized atom has a vacancy in its atomic structure which makes it unstable. To fill this vacancy, an electron from an outer shell can make a radiative transition, whereby the energy of the emitted photon matches the energy difference between the initial and final discrete states. This process is called fluorescence (Kaastra et al. (2008) and references there). The probability of a shell filled by radiative transition is called fluorescent yield Y. For example, for the K-shell, an expression of this yield is given by

$$Y_Z^K = \frac{N_K}{n_{vK}} \tag{1.16}$$

where N_K resembles the number of emitted K-shell X-ray photons, n_{vK} is the number of primary vacancies and Z is the atomic number (Kembhavi & Narlikar, 1999, after Bambynek et al.). Regarding the existence of sub-shells makes the equation more complicated (see Dyson (1990), Kembhavi & Narlikar (1999) for details). The product of the iron abundance and the fluorescent yield is the highest of all elements that can usually be found in astronomical sources (Kembhavi & Narlikar, 1999).

1.3.5 Recombination

As we have seen above, photons can release electrons from atoms therefore transforming the hit atom into an ion. The reverse process, where a free electron is captured by an ion and a photon is emitted, is called recombination (Padmanabhan, 2000). The cross section of radiative recombination can be calculated by the Milne-relation:

$$\sigma_{\text{rr}}(v) = \frac{E^2 g_n \sigma_{\text{phot}}(E)}{m_{\text{e}}^2 c^2 v^2} \tag{1.17}$$

with g_n is the statistical weight of the quantum level to where the electron is captured (Kaastra et al., 2008). Assuming a Maxwell distribution gives recombination coefficients of

$$R_n \sim T^{-\frac{1}{2}},\ \mathrm{k}T \ll E_{\text{bind}} \tag{1.18}$$

and

$$R_n \sim \ln(\frac{E_{\text{bind}}}{\mathrm{k}T}) T^{-\frac{3}{2}},\ \mathrm{k}T \gg E_{\text{bind}}\ , \tag{1.19}$$

which shows that for $T \to 0$ the recombination coefficient diverges, while it is virtually zero for $T \to \infty$ (Kaastra et al., 2008). This approximation shows that in cool plasmas we will mainly find recombination and hot plasmas will predominantly appear ionized.

Figure 1.3: Radio emission of Centaurus A (`http://www.scienceimage.csiro.au/mediarelease/mr09-111.html`). The composite picture shows the size of Centaurus A's radio emission in comparison to the size of the moon in the sky.)

Dielectronic recombination describes a process, where a free electron is caught by an ion, but simultaneously excites another electron. Since this state is not stable the process will be followed by radiative stabilization (Kaastra et al., 2008).

1.3.6 Line emission

Whenever an atom or ion is brought into an excited state it can emit line photons, and the probability for this process is given by

$$P_{ij} = A_{ij} n_j \,, \tag{1.20}$$

where j is the excited state, i is the lower energy level (or ground state), A_{ij} is the spontaneous transition probability, and P_{ij} is the total line power (Kaastra et al., 2008).

1.4 Centaurus A

Centaurus A, located in the Southern Hemisphere, is a radio-loud AGN and one of the best studied sources in this scientific field thanks to its proximity of ~ 3.8 Mpc (Rejkuba, 2004). Its elliptical host galaxy NGC 5128 was discovered in 1826 by James Dunlop (Dunlop, 1828) and Hubble found line emission in the source (Hubble, 1922), but it took until the rise of radio astronomy until scientists had a closer look at Centaurus A. Its immensely extended radio emission has made it the object of various radio studies (see figure 1.3). Centaurus A is partly covered by an optically dark dust lane (see Fig. 1.4, Israel, 1998). Baade & Minkowski (1954) were the first to suggest Centaurus A / NGC 5128 of being a merger of two galaxies, which is


Figure 1.4: *Left*: Centaurus A as seen at optical wavelengths (http://apod.nasa.gov/apod/ap120404.html). Clearly visible is the dust lane, which was first seen by Herschel, 1847. *Right*: Centaurus A in X-rays (http://www.nasa.gov/mission_pages/chandra/multimedia/centaurus-2014.html)

still the general accepted explanation for the source's AGN activity. This activity is powered by a supermassive black hole at the center of the galaxy with a mass of $M_{\mathrm{BH}} = (5.5 \pm 3.0) \times 10^7 M_\odot$ (Cappellari et al., 2009). The X-ray emission of Centaurus A was first discovered by Bowyer et al. (1970). It is believed to be caused by inverse Compton scattering of low energy photons and to be obscured by the dust lane (Israel, 1998). The X-ray spectrum up to $\sim 10\,\mathrm{keV}$ mainly consists of two components: a hard (nuclear?) component which is strongly absorbed, and one in the soft band associated with soft and diffuse emission (Fukazawa et al., 2011, Markowitz et al., 2007). The source's jet shows several knots (Kraft et al., 2002, Hardcastle et al., 2003).

1.4.1 Absorption

Centaurus A is strongly absorbed in the line of sight (Tucker et al., 1973). The origin of the absorption column is possibly a dusty torus surrounding the accretion disk (Evans et al. (2004), Wozniak et al. (1998) and references within). Rivers et al. (2011) showed that the N_{H} column is highly variable and explained this variability with a clumpy torus model. The general idea is that the torus surrounding the accretion disk consists of clumps of material rather than being homogenous. As the torus is also moving, the positions of such clumps change with respect to our line of sight, such that we observe an increasing column density whenever a clump appears between us and the source. A simulation of this model can be found at http://www.nasa.gov/content/goddard/rxte-reveals-the-cloudy-cores-of-active-galaxies/.

2 X-ray analysis of Centaurus A

2.1 Suzaku

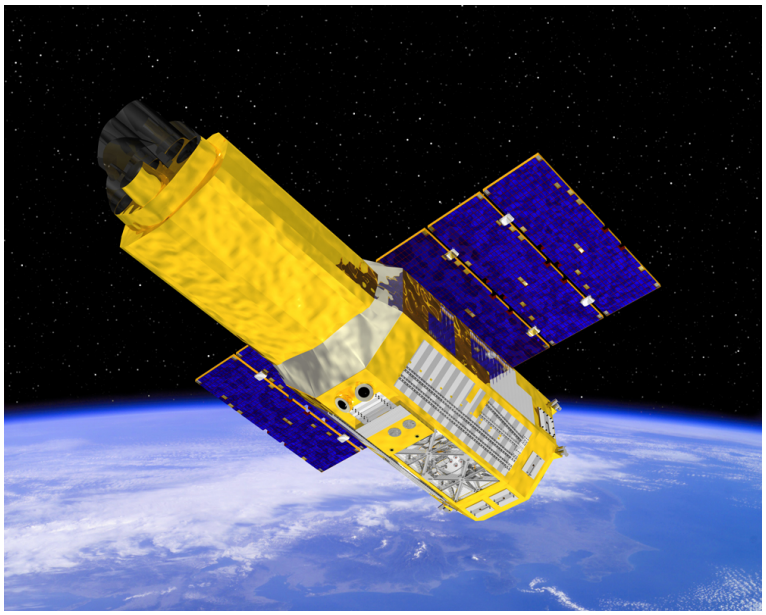

Figure 2.1: An artist's impression of the *Suzaku* satellite (`http://www.astro.isas.jaxa.jp/~oonuki/gallery/Snapshots/index.html`)

Suzaku, a primarily Japanese X-ray mission, is maintained by the Institute of Space and Astronautical Science (ISAS, Japan) in collaboration with the NASA[1] Goddard Space Flight Center (USA). The Suzaku spacecraft, launched in July 2005, hosts four instruments: the X-ray imaging spectrometer (XIS), the hard X-ray detector (HXD), the X-ray telescope (XRT) and the X-ray spectrometer XRS, which unfortunately failed shortly after launch.

The XIS instrument consists of four CCD spectrometers (XIS0 - XIS3), with one being back-illuminated while the others are front-illuminated. XIS2 was damaged in November 2006. The energy range is from 0.2 keV to 12 keV, but due to background issues useful data can only be obtained between 0.5 keV and 10 keV. For detailed information, see Koyama et al. (2007).

A point spread function (PSF) describes how a detector responds to a point source. For each of the three remaining *Suzaku*/XIS detectors the corresponding PSF and a resulting example image is shown in Fig. 2.4.

[1] National Aeronautics and Space Administration

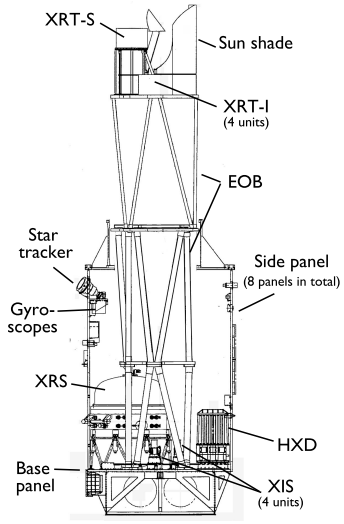

Figure 2.2: Cross section of the *Suzaku* satellite (Mitsuda et al., 2007)

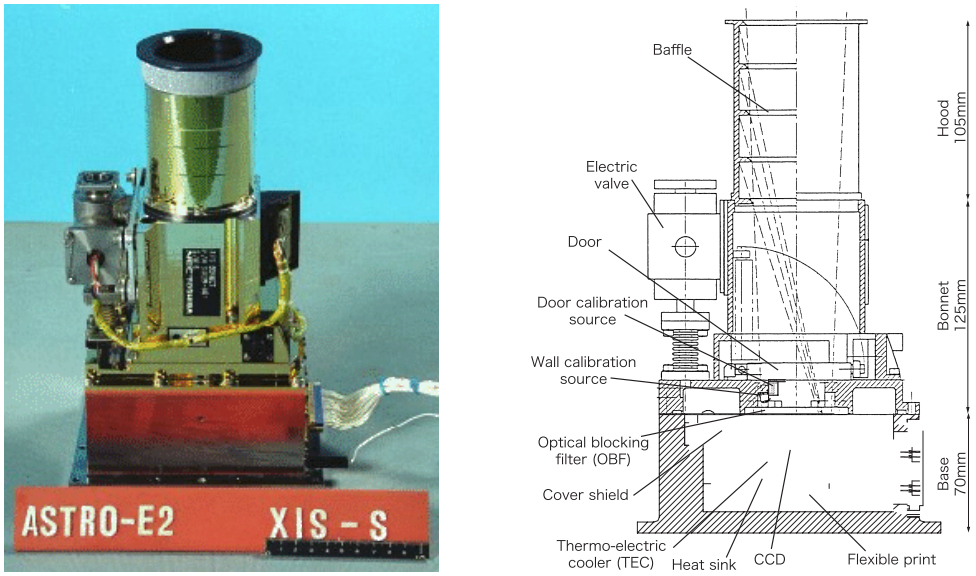

Figure 2.3: *Left*: One of the XIS sensors (`http://www.astro.isas.jaxa.jp/suzaku/doc/suzaku_td/node10.html`) *Right*: Cross section of the XIS sensor (Koyama et al., 2007)

2.2 Analysis with Suzaku

Centaurus A was observed by *Suzaku* most recently in August 2013 for 10.7 ks with XIS in 3 × 3 mode, as well as with HXD. An analysis of the data obtained by the XIS instrument is shown below.

First, the data were prepared with `suzprepare`, which reprocessed the unfiltered data and applies the recent calibration from the *Suzaku* team. Second, extraction regions of 90 arcsec radius and background regions were defined, and data from all three XIS detectors were extracted. The used routine also builds response files for each detector. Details of the extraction scripts can be found at `http://heasarc.gsfc.nasa.gov/docs/suzaku/analysis/abc/node7.html`.

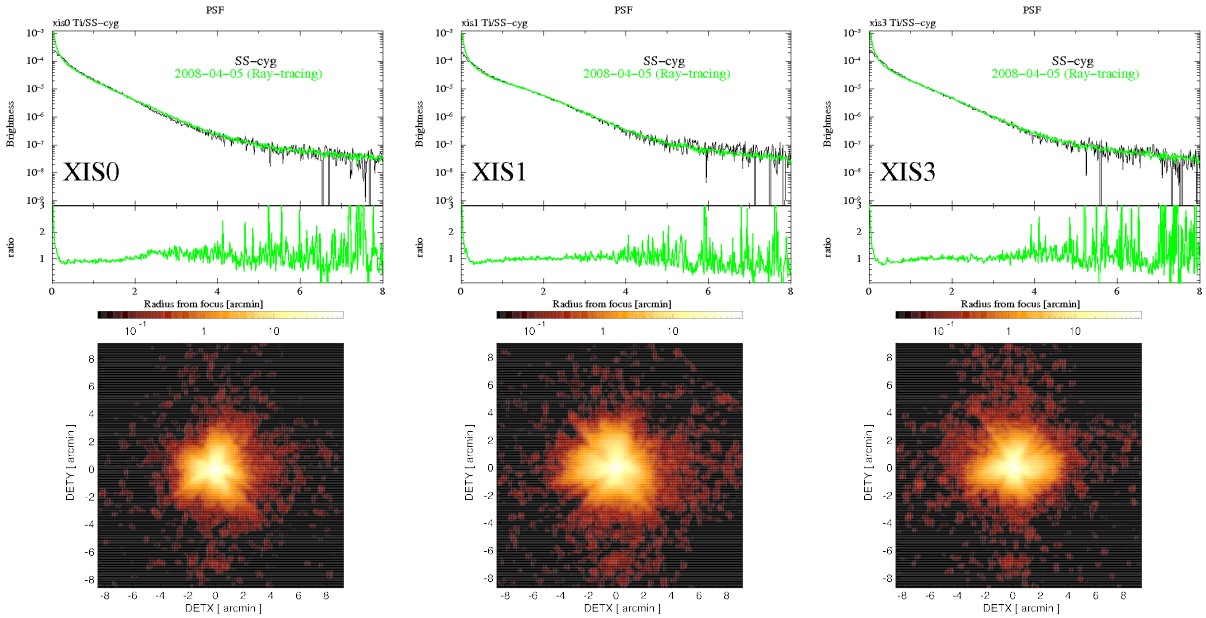

Figure 2.4: PSF of the three *Suzaku*/XIS detectors (`http://www.astro.isas.jaxa.jp/suzaku/doc/suzaku_td/node9.html`).

The XIS count rate was 5−6 counts s^{-1} which is below the limit for pileup ($\sim$ 12.5 counts s^{-1}). The energy ranges 1.72-1.88 keV and 2.19-2.37 keV were ignored due to calibration issues of the Silicon and Gold edges of the detectors (Nowak et al., 2011). Adding the spectral channels and binning the data to a signal-to-noise ratio of at least 5, meaning a minimum of 25 photons in one bin, ensures the validity of using χ^2 statistics. Only data between 0.5 and 10 keV have been used for fitting due to insufficient data quality of the XIS CCDs below and above this energy range. For details of fit modelling in ISIS, see Hanke (2007). Due to the numerous already existing X-ray analyses of Centaurus A and its well-known varying coverage characteristics, this work focuses mainly on two fitting models. The first one is a partial covering model with an Iron line:

```
tbnew_simple*(powerlaw*(egauss+(1-constant)+constant*tbnew_simple_z))
```

The partial coverer consists of two absorbing components, `tbnew_simple` and `tbnew_simple_z` by Wilms et.al (`http://pulsar.sternwarte.uni-erlangen.de/wilms/research/tbabs/`), a constant which is reflecting the covering fraction and a powerlaw component. `tbnew_simple` was used here to take into account absorption of radiation from Centaurus A by material in our own galaxy in the direction of the source. The N_{H}-parameter of the neutral hydrogen column density has therefore been set to a fixed value of 0.0809×10^{22} cm^{-2}, which was obtained from NASA's N_{H}-calculator (`http://heasarc.gsfc.nasa.gov/cgi-bin/Tools/w3nh/w3nh.pl`). `tbnew_simple_z` contains a redshift parameter z as well as another value of N_{H} which here describes the intrinsic column density of neutral hydrogen. The second model is a modified version of the best fit by Markowitz et al. (2007):

```
tbnew_simple*(zpowerlw+zgauss+tbnew_simple_z*powerlaw+tbnew_simple_z*powerlaw)
```

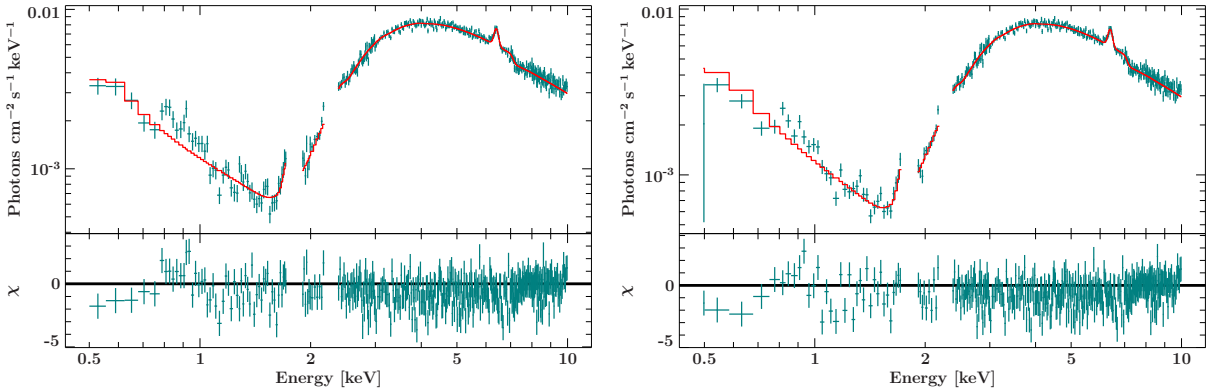

Figure 2.5: *Suzaku* spectrum of Centaurus A. The left image shows a fitted partial covering model, the right image shows a fitted model similar to the one used by Markowitz et al. (2007). Detector edges were cut off to fit the model properly.

This model consists again of `tbnew_simple` for galactic absorption, `zpowerlw` which is associated with the (kiloparsec) jet and two absorbed powerlaws associated with a primary and secondary absorber. As one can see in figure 2.5, the big hump at $\sim$ 2 - 10 keV is well described in both models, but there are some residuals leftover below 2 keV.

In an analysis of a *Suzaku* observation of Centaurus A in 2005, Markowitz et al. (2007) discuss the existence of several emission lines. A model very similar to the one used in the 2007 Centaurus A analysis was tested in the next step. This model describes the spectrum well, even a closer look at the soft X-ray emission below 2 keV reveals that the model still seems to hold (see table 2.2). The emission lines in the soft X-rays do also appear in the spectrum of 2013 (see Fig. 2.6).

To gather information about the material surrounding the black hole, it is important to clarify the nature of emission lines in energies below 2 keV. An overview of possible prominent line energies and their matching elements is given in table 2.1. Finding forbidden lines in the material of an AGN means photoionization processes within, since forbidden transitions are statistically rare and hence only occur in cold, low density gas. In contrast, when material is hot and dense, particles collide more often such that forbidden transitions vanish and we find only resonance lines, which is the case, when collisional ionization dominates the processes in the gas.

Although Fukazawa et al. (2011) analyzed three *Suzaku* observations of Centaurus A from 2009, they did not investigate the nature of soft X-ray emission lines in the diffuse region. Therefore, this work does not refer to their model in detail.

Suzaku does not allow us neither to resolve the emission lines present in the spectrum of Centaurus A (due to its insufficient resolution in low X-rays), nor to determine the origins of different X-ray components or analyze emission regions separately. To solve the latter problem, we used data from the *Chandra* satellite with a much better angular resolution. Details of this analysis are described in the following section.

Table 2.1: Soft X-ray emission lines
(`http://mamacass.ucsd.edu/~agm/alllines.html`)

Element	$E_{\rm line}$ keV	Line type
O VII	0.561	forbidden
O VII	0.568	intercombination
O VII	0.574	resonance
O VIII	0.653	Ly α
Fe XVII	0.726	3s-2p
Fe XVII	0.826	3d-2p
Ne IX	0.905	forbidden
Ne IX	0.915	intercombination
Ne IX	0.922	resonance
Ne X	1.022	Ly α
Mg XI	1.331	forbidden
Mg XI	1.343	intercombination
Mg XI	1.352	resonance

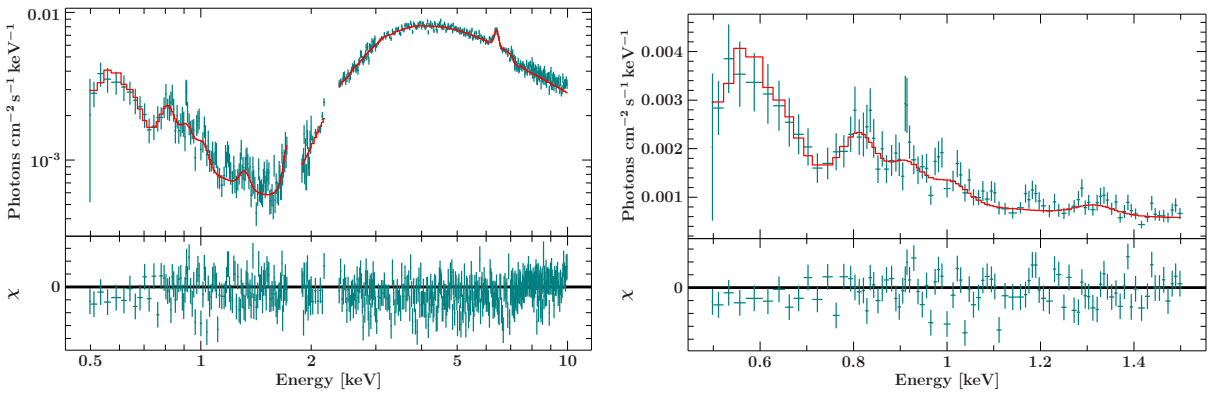

Figure 2.6: Soft emission lines included in the model.

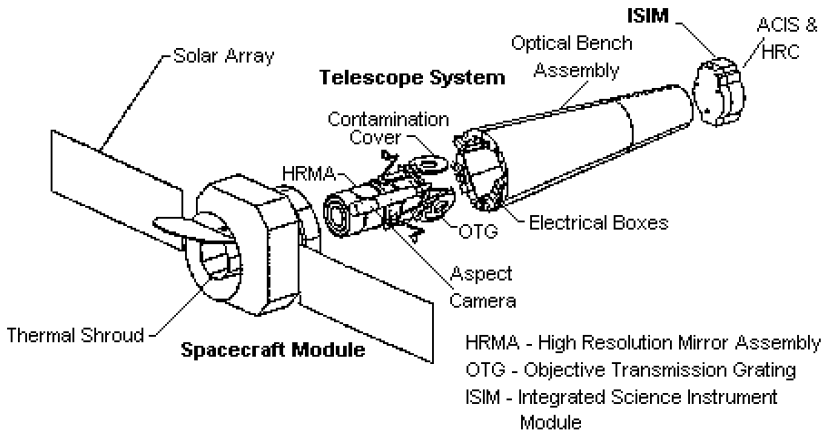

Figure 2.8: Parts and scientific instruments of *Chandra* (Weisskopf et al., 2002)

2.3 Chandra

Figure 2.7: An artist's impression of the *Chandra* satellite (`http://chandra.harvard.edu/resources/illustrations/craftIllustrations.html`)

The *Chandra* X-ray Observatory, operated by NASA, was launched in July 1999. It has several science instruments onboard: the High Resolution Camera (HRC), the Advanced CCD Imaging Spectrometer (ACIS) and two high resolution spectrometers, the High Energy Transmission Gration Spectrometer (HETGS) and the Low Energy Transmission Grating Spectrometer (LETGS). The ACIS instrument is sensitive to X-rays between 0.2 keV and 10 keV. For details see Garmire et al. (2003), Weisskopf et al. (2002) and the *Chandra* website (`http://cxc.harvard.edu/cal/`).

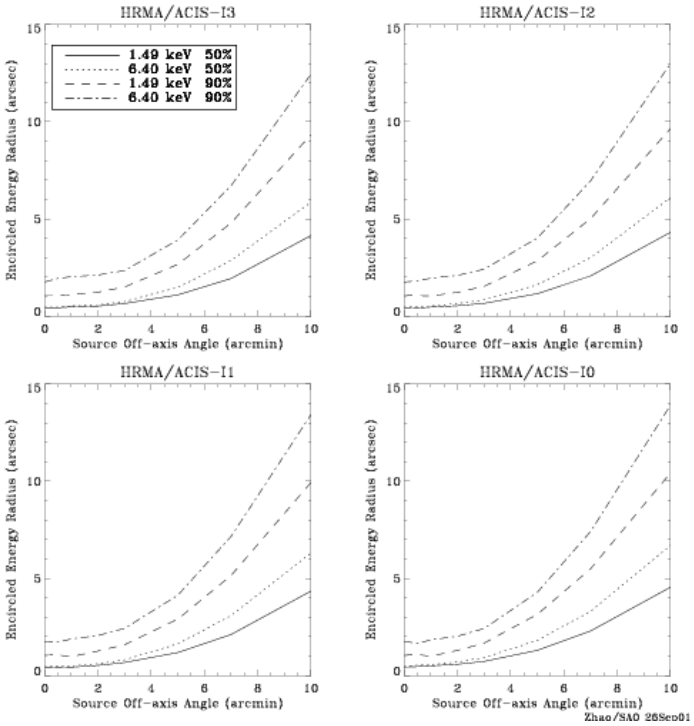

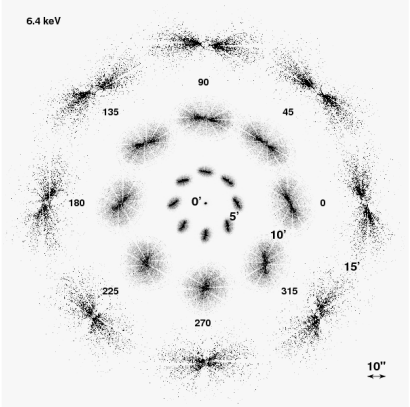

Figure 2.9: *Left:* PSF of *Chandra*/ACIS. *Above:* Simulated image showing how a source would appear in ACIS depending on the off-axis angle (5', 10' and 15'). (`http://cxc.harvard.edu/proposer/POG/html/HRMA.htm`)

Figure 2.10: *Left: Suzaku*/XIS3 image of the observation in 2013 August. The white circle shows the extraction region used for analyzing the source's spectrum ($r = 90$ arcsec). *Right: Chandra*/ACIS image of the observation of Centaurus A in 2009 September. The white circle again shows the extraction region, which is the same size used for extracting the *Suzaku* spectrum.

2.4 Analysis with Chandra

Centaurus A is observed by *Chandra* frequently and data from observations are available via the *Chandra* data archive (`http://cxc.harvard.edu/cda/`). I analyzed a *Chandra*/ACIS observation from 2009 with an exposure of 50 ks. The data from were reprocessed using `chandra_repro`, which creates event and bad pixel files. A circular extraction region with $r = 90$ arcsec was used to make the spectrum comparable to the *Suzaku* spectrum and a background region was created. Then data were extracted with the `specextract` tool, producing source spectra and response files. The CIAO scripts can be found at `http://cxc.harvard.edu/ciao/`.

First, the parameters from the best fit of the *Suzaku* data were compared to a *Chandra*

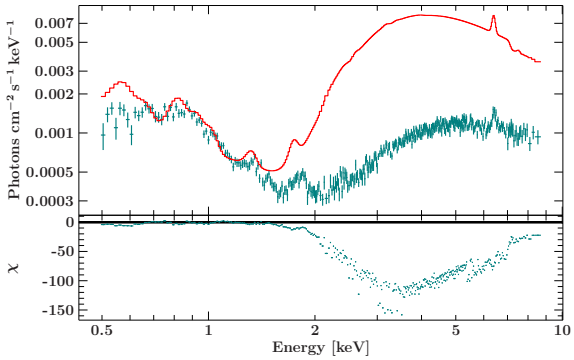

Figure 2.11: Comparison of *Suzaku* model to *Chandra* spectrum.

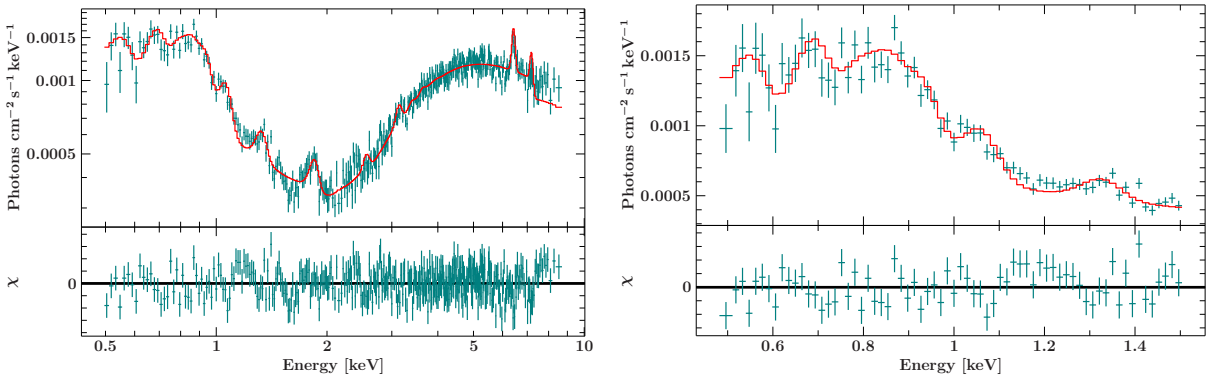

Figure 2.12: *Chandra* spectrum fitted with absorbing components and lines in the soft X-rays.

spectrum (see Fig. 2.11). The soft emission fits quite well even though X-ray emission at $\sim$ 0.5 keV is a bit higher in *Suzaku*. However, the hard X-ray emission does not fit at all, which can be explained with the variability of the source in the hard X-rays (Müller et al., submitted). Fitting the model to the spectrum shows that *Chandra's* energy resolution is slightly worse than *Suzaku's*. The emission lines can be fitted, but do not appear as clear as in the *Suzaku* spectrum (see Fig. 2.12). However, thanks to *Chandra's* excellent PSF, one can distinguish better than with *Suzaku* between different emission regions, e.g., core, jet and diffuse emission. A comparison of X-ray emission of those three regions is shown in Fig. 2.13.

The core of Centaurus A emits almost only hard X-rays. Soft X-ray emission is due to absorption of the core by the diffuse material surrounding it. This core emission spectrum can be fitted with an absorbed powerlaw (Fig. 2.14). The source's jet can be fitted well with a powerlaw (Fig. 2.15).

2.4.1 Diffuse emission

Analyzing the diffuse emission region in Centaurus A was very surprising. Once having cut out the regions of the core and jet, one would expect no hard X-ray emission to be left. However, as one can see in Fig. 2.13, the diffuse material of the source also emits energy above 3 keV. How the diffuse region looks like above certain energy thresholds is shown in Fig. 2.18. The model including the soft emission lines fits the spectrum of the diffuse emission very well (Fig. 2.16).

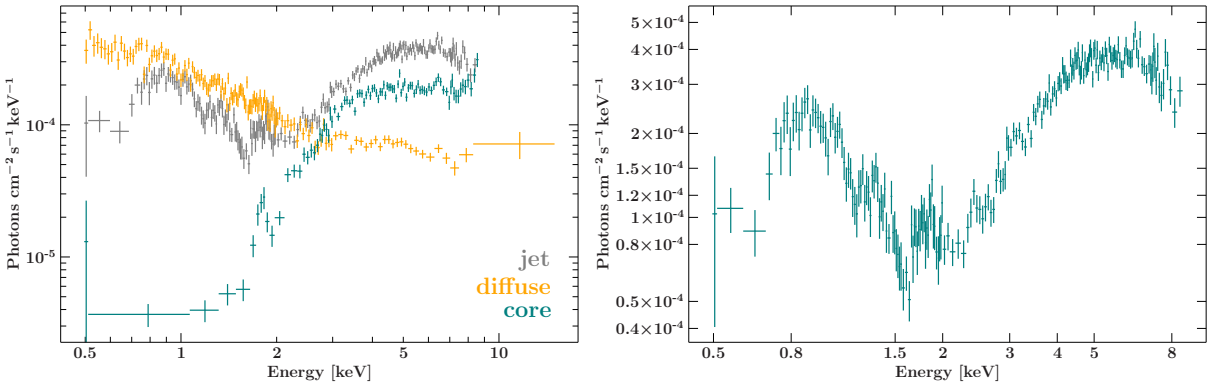

Figure 2.13: *Left:* Compared X-ray spectra of different emission regions of Cen A. Emission from the core is shown in orange, jet emission is blue and gray shows emission from the diffuse region. *Right:* Cen A's diffuse emission.

Table 2.2: Comparison of the two *Suzaku* observations and the *Chandra* observation of Centaurus A. The parameters from 2005 are those of the best fit model as discussed in (Markowitz et al., 2007).

Parameter	2005	2009	2013
χ^2 / dof	9529.9 / 9142	480.4753 / 7	2671.782 / 7
$\Gamma_{1,2}$	$1.817^{+0.023}_{-0.010}$	1.244 ± 0.006	$1.7547^{+0.0026}_{-0.0025}$
PL_1 normalization	$0.111^{+0.001}_{-0.002}$	$(1.80 \pm 0.08) \times 10^{-3}$	0.1403 ± 0.0008
$N_{H_1}[10^{22}\,cm^2]$	$14.7^{+0.3}_{-0.2}$	23^{+15}_{-18}	14.32 ± 0.10
PL_2 normalization	0.021 ± 0.003	0.01163 ± 0.00012	0.0448 ± 0.0010
$N_{H_2}[10^{22}\,cm^2]$	70^{+11}_{-7}	$24.64^{+0.28}_{-0.27}$	$22.5^{+0.7}_{-0.6}$
Γ_3	$1.31^{+0.08}_{-0.10}$	$1.220^{+0.026}_{-0.025}$	$1.33^{+0.12}_{-0.11}$
PL_3 normalization	$(7.0^{+0.6}_{-0.3}) \times 10^{-4}$	$(7.04 \pm 0.11) \times 10^{-4}$	$(7.3 \pm 0.4) \times 10^{-4}$

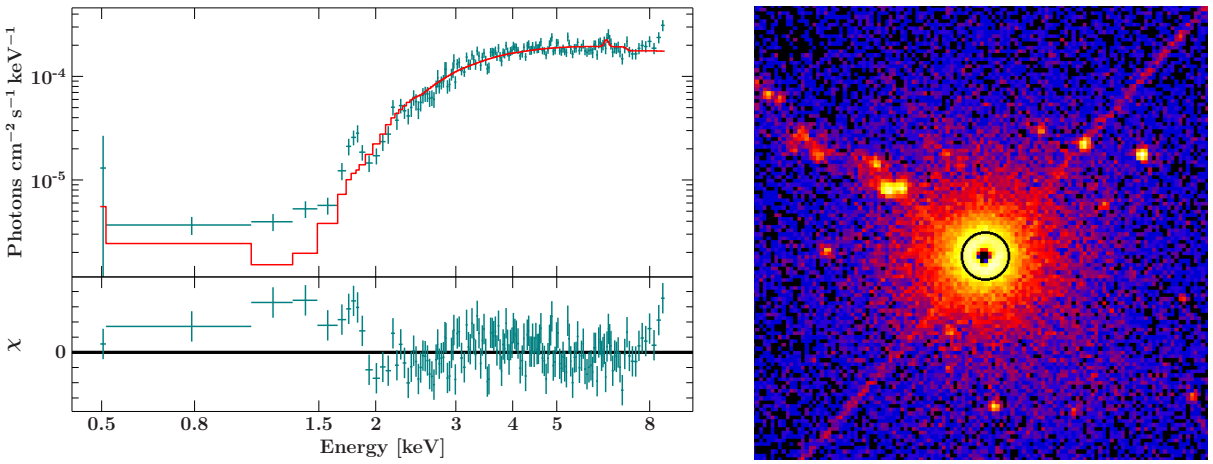

Figure 2.14: *Left:* The spectrum of Centaurus A's core region can be fitted with an absorbed powerlaw. *Right:* The black circle shows the extraction region which was used for extracting the jet spectrum ($r = 3.05$ arcsec).

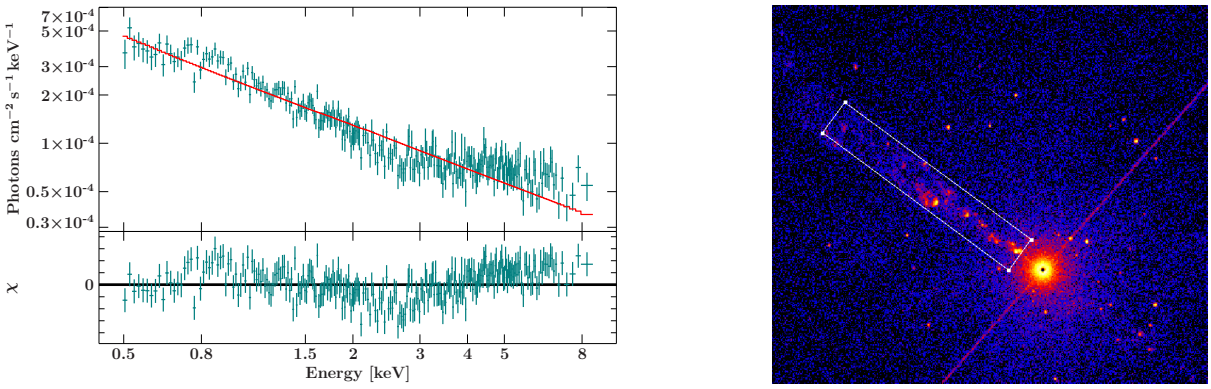

Figure 2.15: *Left:* The spectrum of Centaurus A's jet is well represented with a powerlaw. *Right:* The white box shows the extraction region which was used for extracting the jet spectrum (106.9 arcsec × 17.6 arcsec).

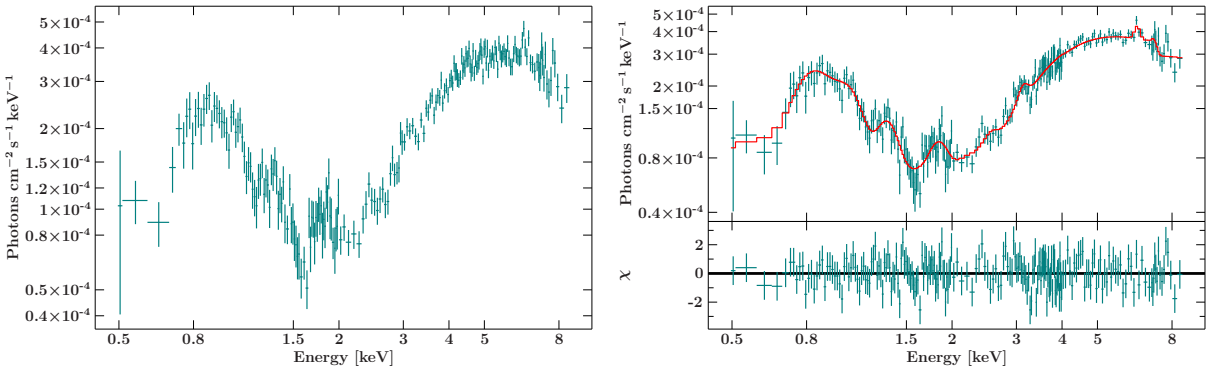

Figure 2.16: Diffuse emission of Centaurus A

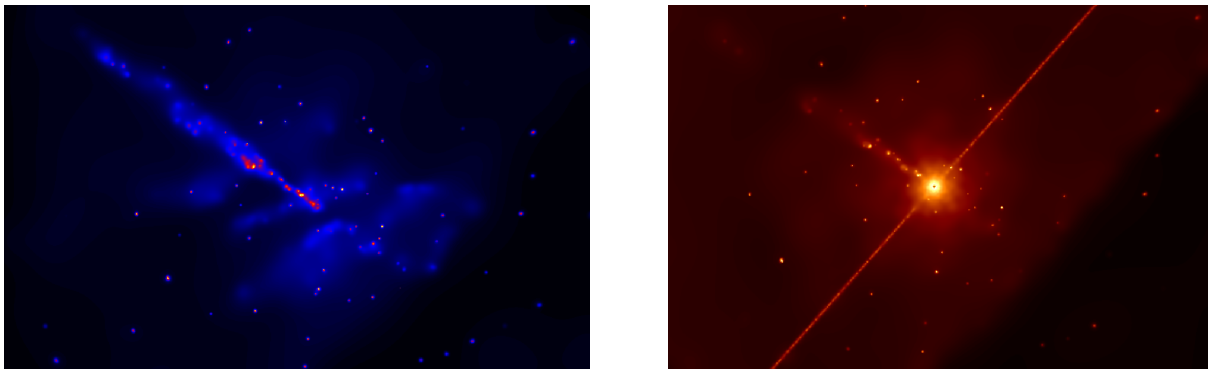

Figure 2.17: *Left*: *Chandra*/ACIS image of Centaurus A showing only X-ray emission $\leqslant 2$ keV. Clearly visible are the jet and the extended diffuse emission. *Right*: The same observation showing only X-ray emission $\geqslant 2$ keV. The extended hard emission is surprising, because obviously it is emitted not only by the core (which would be only a point source). Both pictures have been smoothed with the CIAO tools.

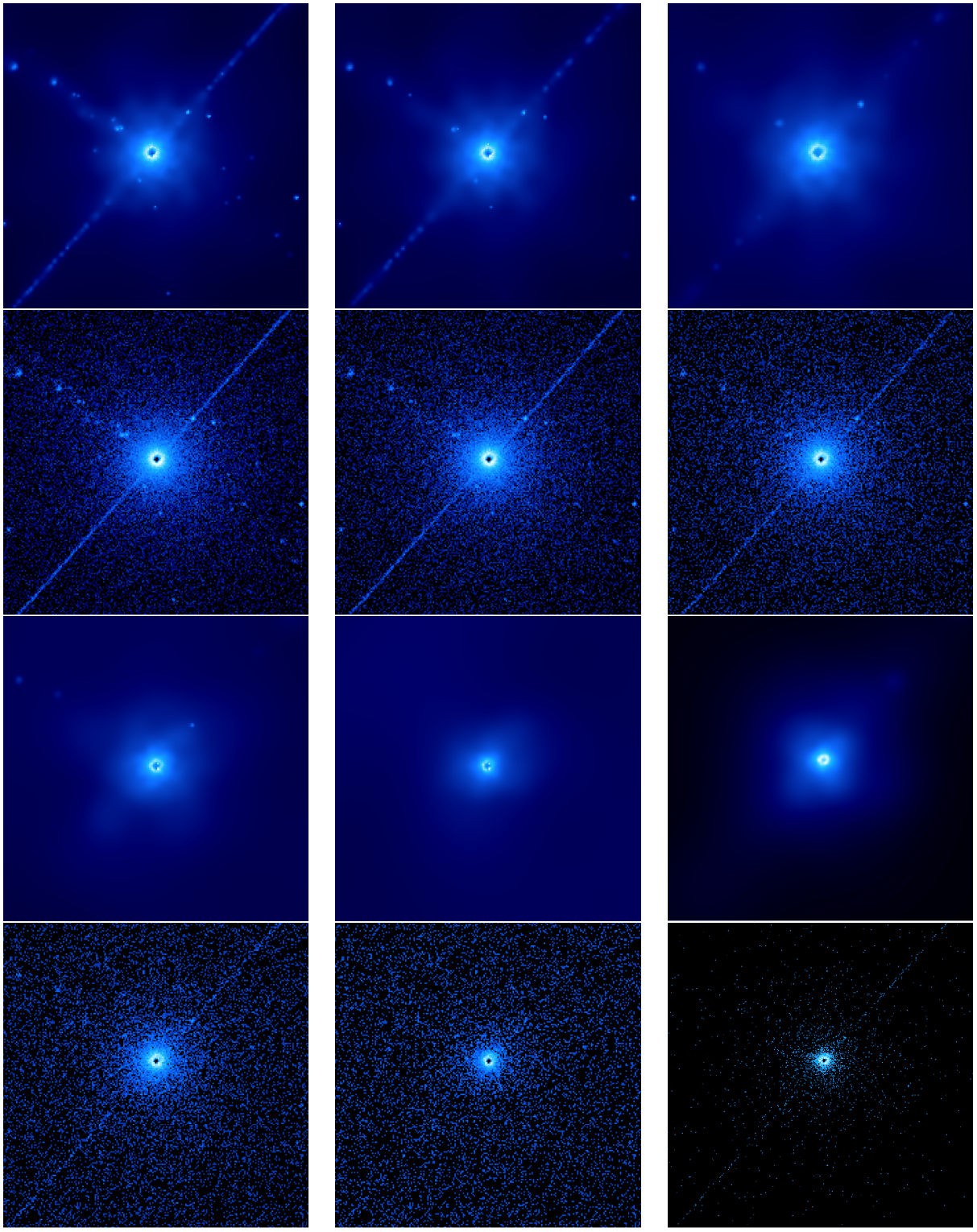

Figure 2.18: These figures show the hard X-ray emission of Centaurus A. The top three images from left to right show the emission above 3, 4 and 5 keV. The line below shows the corresponding unsmoothed images. The third line shows from left to right the emission above 6 and 7 keV as well as a map for the iron line (energy range between 6.3 and 6.6 keV). The streak in some of the pictures is a detector feature.

3 Results and Outlook

The model by Markowitz et al. (2007) fits the *Suzaku* spectrum remarkably well. The presence of emission lines in the diffuse emission region of Centaurus A can be confirmed, even though the energy resolution of both the XIS and the ACIS instruments does not allow us to resolve the emission lines completely in order to distinguish between possible ionization models. Furthermore, soft X-rays are exclusively emitted from the diffuse region and the jet.

The jet emission can be fitted with a powerlaw only, which can be explained with synchrotron radiation of the accelerated particles in the jet. Showing no absorption apart from galactic, the diffuse absorber of Centaurus A seems to have the shape of a disc.

The N_{H} shows a high variability. This can confirm the model of a clumpy torus within the line of sight (Rivers et al., 2011). The varying N_{H} column might also be the reason for the unusual powerlaw properties of the spectrum from 2009. Variability of absorption strongly effects the powerlaw when changing and vice versa.

Further investigations should concentrate on analyzing the soft emission lines. Because of the limited energy resolution of CCD detectors, gratings instruments must be used. A proposal for a 100 ks *Chandra*/LETGS observation of Centaurus A was submitted in March 2014. Assuming that this observation will be performed, we can analyze the emission lines and constrain temperature and density of the diffuse material surrounding the black hole. Another task for further studies is the investigation of the origin of the hard X-rays in the diffuse region, as one would assume the core being by far the main source of hard X-rays.

As we have seen above, the hard X-ray emission of Centaurus A changes violently. This variability is already discussed in Müller et al. (submitted) and may be topic of ongoing studies.

4 | Summary

This work presented the analyses of two observations of Centaurus A and their comparison to previous investigations. Although there have been various studies of the source in all wavelengths, the emission processes and features of the diffuse material are not yet understood. This work showed there is evidence for emission lines in the soft X-rays. I also showed that the core of Centaurus A does not emit soft X-rays, while the diffuse material emits radiation both in the soft and the hard X-ray band. The jet of Centaurus A is only absorbed by our own galaxy, which implies a disc shape of the diffuse emission region. However, with the existing data we cannot resolve the emission lines satisfactorily, which leads to the need of gratings observations.

References

Baade W., Minkowski R., 1954, The Observatory 74, 130
Bambynek W., Crasemann B., Fink R.W., et al.,
Bowyer C.S., Lampton M., Mack J., de Mendonca F., 1970, Astrophys. J., Lett. 161, L1
Cappellari M., Neumayer N., Reunanen J., et al., 2009, MNRAS 394, 660
Dunlop J., 1828, Royal Society of London Philosophical Transactions Series I 118, 113
Dyson N.A., 1990, X-rays in Atomic and Nuclear Physics
Evans D.A., Kraft R.P., Worrall D.M., et al., 2004, ApJ 612, 786
Fukazawa Y., Hiragi K., Yamazaki S., et al., 2011, ApJ 743, 124
Garmire G.P., Bautz M.W., Ford P.G., et al., 2003, In: Truemper J.E., Tananbaum H.D. (eds.) X-Ray and Gamma-Ray Telescopes and Instruments for Astronomy., Vol. 4851. Society of Photo-Optical Instrumentation Engineers (SPIE) Conference Series, p.28
Hanke M., 2007, Diploma thesis, Astronomical Institute of the University of Erlangen-Nuremberg
Hardcastle M.J., Worrall D.M., Kraft R.P., et al., 2003, ApJ 593, 169
Herschel, Sir J.F.W., 1847, Results of astronomical observations made during the years 1834, 5, 6, 7, 8, at the Cape of Good Hope; being the completion of a telescopic survey of the whole surface of the visible heavens, commenced in 1825
Hubble E.P., 1922, ApJ 56, 162
Israel F.P., 1998 8, 237
Kaastra J.S., Paerels F.B.S., Durret F., et al., 2008, Space Sci. Rev. 134, 155
Karzas W.J., Latter R., 1961, ApJS 6, 167
Kembhavi A.K., Narlikar J.V., 1999, Quasars and active galactic nuclei : an introduction
Koyama K., Tsunemi H., Dotani T., et al., 2007, PASJ 59, 23
Kraft R.P., Forman W.R., Jones C., et al., 2002, ApJ 569, 54
Krolik J.H., 1999, Active galactic nuclei : from the central black hole to the galactic environment, Princeton University Press
Markowitz A., Takahashi T., Watanabe S., et al., 2007, ApJ 665, 209
Mitsuda K., Bautz M., Inoue H., et al., 2007, PASJ 59, 1
Nowak M.A., Hanke M., Trowbridge S.N., et al., 2011, ApJ 728, 13
Padmanabhan P., 2000, Theoretical astrophysics. Vol.1: Astrophysical processes
Rejkuba M., 2004, A&A 413, 903
Rivers E., Markowitz A., Rothschild R., 2011, Astrophys. J., Lett. 742, L29
Rybicki G.P., Lightman A.P., 1979, Radiative processes in astrophysics, Wiley
Schneider P., 2006, Einführung in die extragalaktische Astronomie und Kosmologie, Springer
Shu F.H., 1991, The physics of astrophysics. Volume 1: Radiation.
Tucker W., Kellogg E., Gursky H., et al., 1973, ApJ 180, 715
Urry C.M., Padovani P., 1995, PASP 107, 803
Weisskopf M.C., Brinkman B., Canizares C., et al., 2002, PASP 114, 1
Wilms J., 2012, Astrophysical Radiation Processes
Wozniak P.R., Zdziarski A.A., Smith D., et al., 1998, MNRAS 299, 449

Acknowledgements

First of all I want to express a special word of thanks to my supervisor Jörn Wilms and to both Felicia Krauß and Cornelia Müller, who supported me with their great knowledge and advice.

Furthermore, I want to thank Sebastian Falkner, for the fruitful discussions, and not least for the moral support through all the time.

I want to thank Alex Markowitz for his great support and advice concerning all questions of AGN and Centaurus A.

I want to thank my supervisor Matthias Kadler from Würzburg and the whole Remeis-Observatory working group, especially Tobias Beuchert, Thomas Dauser and Matthias Kühnel for all the help throughout the process of working on this bachelor thesis.

I want to express my thanks also to Florian Horn and Johannes Hölzl for their motivation.

Finally, I want to thank my family for their support.

This research has made use of ISIS[1] functions provided by ECAP/Remeis observatory and MIT .

[1] Interactive Spectral Interpretation System

Erklärung

Hiermit bestätige ich, dass ich diese Arbeit selbstständig und nur unter Verwendung der angegebenen Hilfsmittel angefertigt habe.

Bamberg, den 14.04.2014